Journal of Applied Physics

# Experimental and simulation studies on temporal evolution of chemically etched Si surface: Tunable light trapping and cold cathode electron emission properties

Cite as: J. Appl. Phys. **125**, 164302 (2019); https://doi.org/10.1063/1.5079481
Submitted: 31 October 2018 . Accepted: 03 April 2019 . Published Online: 23 April 2019

Ranveer Singh, Safiul Alam Mollick, Mahesh Saini, Puspendu Guha, and Tapobrata Som

Journal of Applied Physics ARTICLE scitation.org/journal/jap

# Experimental and simulation studies on temporal evolution of chemically etched Si surface: Tunable light trapping and cold cathode electron emission properties

Cite as: J. Appl. Phys. **125**, 164302 (2019); doi: 10.1063/1.5079481
Submitted: 31 October 2018 · Accepted: 3 April 2019 ·
Published Online: 23 April 2019



Ranveer Singh,[1,2] Safiul Alam Mollick,[1,a)] Mahesh Saini,[1,2] Puspendu Guha,[1,2] and Tapobrata Som[1,2,b)]

## AFFILIATIONS

[1]Institute of Physics, Sachivalaya Marg, Bhubaneswar 751 005, Odisha, India
[2]Homi Bhabha National Institute, Training School Complex, Anushakti Nagar, Mumbai 400 085, India

[a)]**Present address:** Department of Physics, Indian Institute of Technology Roorkee, Roorkee 247 667, India.
[b)]**Author to whom correspondence should be addressed:** tsom@iopb.res.in

## ABSTRACT

Anisotropic alkaline etching of single crystalline *p*-Si(100) substrates is carried out for different times (in the range of 30–2400 s). This leads to the formation of randomly distributed pyramidal structures on Si surfaces, as observed from atomic force microscopy (AFM) and scanning electron microscopy images. During early stages of etching, rough surfaces evolve, but for longer etching times, pyramidally textured surfaces (having dimensions in the range of 0.2–2 $\mu$m) are formed. The formation of pyramidal structures is explained in light of simulation studies based on the continuum theory of stress-induced morphological instability. The power spectral density plots extracted from the experimental AFM images and the simulated images show that while the correlation length increases for lower etching times, it gets saturated for higher etching times. These facts corroborate well with our experimental results that reveal increasing pyramidal size with etching time. In addition, we study the temporal evolution of antireflection and field emission properties of such pyramidally textured-silicon substrates in line with their potential use in solar cells and moderate level cold cathode electron emission, respectively. For instance, it is interesting to note that surface reflectance of these pyramidally textured surfaces (formed at higher etching times) can be brought down to as low as 0.4% over a broad spectral range, viz., 300–3000 nm. Likewise, the field emission data show that turn-on potential decreases with increasing etching time (e.g., 2.62 V $\mu m^{-1}$ for an etching time of 1200 s).



## I. INTRODUCTION

Micro/nanostructures of silicon are important for the current semiconductor industry and are considered to be the building blocks for device fabrication in the fields of nanoelectronics,[1] optoelectronics,[2] energy-conversion,[3] energy-storage,[4] as well as biosensor and chemical-sensor.[5] Photovoltaic (PV) devices based on Si micro/nanostructures exhibit higher power conversion efficiency (PCE) in comparison with other devices due to their increased absorption of solar light.[6,7] However, due to the simultaneous enhancement of the recombination of photogenerated charge carriers, these devices may show a low PCE.[6,8] Generally, these micro/nanostructures are grown on *c*-Si wafers[8,9] using lithography,[8] laser modification,[10] reactive ion etching,[11,12] ion-beam modification,[13,14] wet chemical etching,[15–17] and molecular beam epitaxy.[18] In the field of solar energy research, it is important to increase the surface area of micro/nanostructures and maximize the photoabsorption to enhance the performance of a device. Wet chemical etching of semiconducting materials is widely accepted as the most cost-effective route for the fabrication of large area micro/nanostructures.[8,9,11,16,17,19,20] For instance, texturing of *c*-Si substrates by this process is considered to be important for the fabrication of high-efficiency *c*-Si based solar cells where one can grow a variety of structures, viz., microholes, pyramids, triangles, and rectangles.[9,21] The chemical composition

of the etchants, as well as the substrate composition, plays an important role in determining the morphologies evolved by chemical etching.[22]

Among these, pyramidally textured-Si surfaces help reduce the reflection of light over a wide band of spectral range (300–3000 nm)[7,16,17] by enhancing light trapping through multiple reflections. This results in a large number of photogenerated charge carriers.[21] However, Oh *et al.*[6] have shown that due to an enhancement of the surface area of micro/nanostructured devices, the recombination rate of photogenerated carriers increases, leading to a decrease in the PCE.[6] Thus, it is important not only to understand the underlying mechanisms behind the fabrication of pyramidally textured-Si surfaces but also to explore their potential applications. For instance, Saini *et al.* have shown broadband antireflection of light in the case of conformally grown Al-doped ZnO films on chemically prepared pyramidally textured-Si surfaces.[16] On the other hand, Oh *et al.* have shown that the power conversion efficiency of chemically prepared pyramidally textured-Si solar cells can be enhanced as high as 18.6% where $SiN_X$ is used as an antireflection layer.[6] Likewise, Kumar *et al.* have shown that a solar cell fabricated with a $Cu_2O$ overlayer on a *textured*-Si substrate exhibits an eight times higher efficiency compared to the one where the $Cu_2O$ layer is grown on a *pristine*-Si substrate.[7]

It is well known that acidic etching is isotropic where etching takes place from all directions at the same rate and produces isotropic features on a Si surface.[23] Recently, Sana *et al.* have shown isotropic etching of single crystalline-Si surfaces using a mixture of HF, $HNO_3$, and $CH_3COOH$ for different times.[24] On the other hand, alkaline etching is anisotropic and results in geometric shapes bound by perfectly defined crystallographic planes since the rate of etching has a directional dependence.[25] For instance, Peng *et al.* have demonstrated that the formation of ordered silicon nanowire arrays takes place due to a selective and anisotropic etching of Si in a solution of HF and $H_2O_2$.[26] As a matter of fact, in the case of an alkaline etching process, anisotropic solutions of sodium hydroxide (NaOH) or potassium hydroxide (KOH) and isopropyl alcohol (IPA) are used to fabricate highly dense and randomly distributed pyramidal structures (approximately micrometer) on a *c*-Si (100) surface without using any mask.[9,24,27,28] However, potassium contamination from KOH/IPA solution is harmful for microelectronics and also adversely affects photovoltaic devices.[28] In order to fabricate pyramidal structures without any impurity/contamination, NaOH is considered to be an excellent replacement for KOH.[9] To understand the mechanism of chemical etching, several hypotheses have been put forward based on the concept of scaling[29,30] and self-affine behavior of NaOH-etched crystalline-Si surfaces (under various conditions) as studied by Dotto and Kleinke.[31] On the other hand, Kessler *et al.* have explained the texturing process using a percolation model.[29] Likewise, stress-induced roughening is another widely accepted mechanism to account for morphological instability on solid surfaces.[30] In spite of the availability of various models for the texturing mechanism on the Si surface, there is a lack of a generalized approach to understand the texturing dynamics using a continuum equation. Thus, there is a need to study the temporal evolution of these pyramidal structures in terms of their shape, size, and coverage area/number density.

In this paper, we report on the fabrication of self-assembled pyramidal structures on *c*-Si substrates using the anisotropic alkaline etching process with the help of NaOH and IPA for different time durations—ranging from 30 to 2400 s. It is found that with increasing etch time, the average dimension of randomly distributed pyramids on *c*-Si substrates increases from 0.2 $\mu$m to 2 $\mu$m. In addition, we have carried out statistical analysis of the temporal evolution of chemically etched Si surfaces. For instance, using SPIP software[32] we have extracted roughness, power spectral density (PSD), lateral correlation length [$G(r)$], and other relevant parameters to understand the morphological evolution of Si at different etching times. We have also carried out simulation studies on the temporal evolution of morphology on the *c*-Si surface by employing the continuum theory of stress-induced morphological instability. Upon comparing the numerically simulated images with the experimental ones, we observe a close proximity of the two, justifying employment of the present formalism.

In addition, we also show tunability in some of the functional properties of these randomly distributed pyramidal structures, formed under different etching times. For instance, we have measured their surface reflectance which is observed to reduce drastically from ~40% (pristine-Si) to as low as ~0.4% (for an etching time of 2400 s) over the entire spectral range of 300–3000 nm. This low reflectance is attributed to multiple reflections of light caused by the geometrical shape of pyramidal structures.[7] Furthermore, we have measured the cold cathode electron emission property of these pyramidally textured-Si surfaces and found that with increasing etching time, the turn-on potential decreases and can be brought down to as low as 2.62 V $\mu m^{-1}$ for an etch duration of 1200 s. Thus, the present work paves the way to fabricate tailor-made pyramidally textured-Si surfaces which manifest tunable antireflection property as well as cold cathode electron emission with moderate emission current density. These studies will be extremely useful for the fabrication of photovoltaic cells having higher efficiency and silicon-based field emission (FE) devices.

## II. EXPERIMENTAL DETAILS

For the present study, a 500 $\mu$m thick *p*-type Si(100) wafer was cut into several small pieces (area $1 \times 1$ $cm^2$). Prior to chemical etching, the Si substrates were cleaned by trichloroethylene, isopropyl alcohol, acetone, and deionized water (Milli-Q Gradient water purification system, Millipore) for 300 s each using an ultrasonicator. Following this, Si substrates were etched in a 30 wt. % NaOH solution (in $H_2O$) at 348 ± 2 K for 180 s during which both the top and the rear surfaces were cleaned through the removal of 3–4 $\mu$m thick Si from each side. Afterward, controlled chemical etching was executed at 353 ± 2 K for different times starting from 30 to 2400 s in 3 wt. % NaOH solution in the presence of 10% IPA. A schematic diagram of the etching setup is shown in Fig. 1. After completion of the chemical etching, Si substrates were further immersed in 20% HCl for 60 s followed by rinsing in deionized water to remove the Na residues. Finally, they were cleaned in 10% HF for 20 s to remove the native $SiO_x$ layer and neutralize the residual chemicals which was followed by multiple washing in deionized water.[7]

Morphological evolution of Si surfaces was studied by field emission gun-based scanning electron microscopy (FEGSEM,

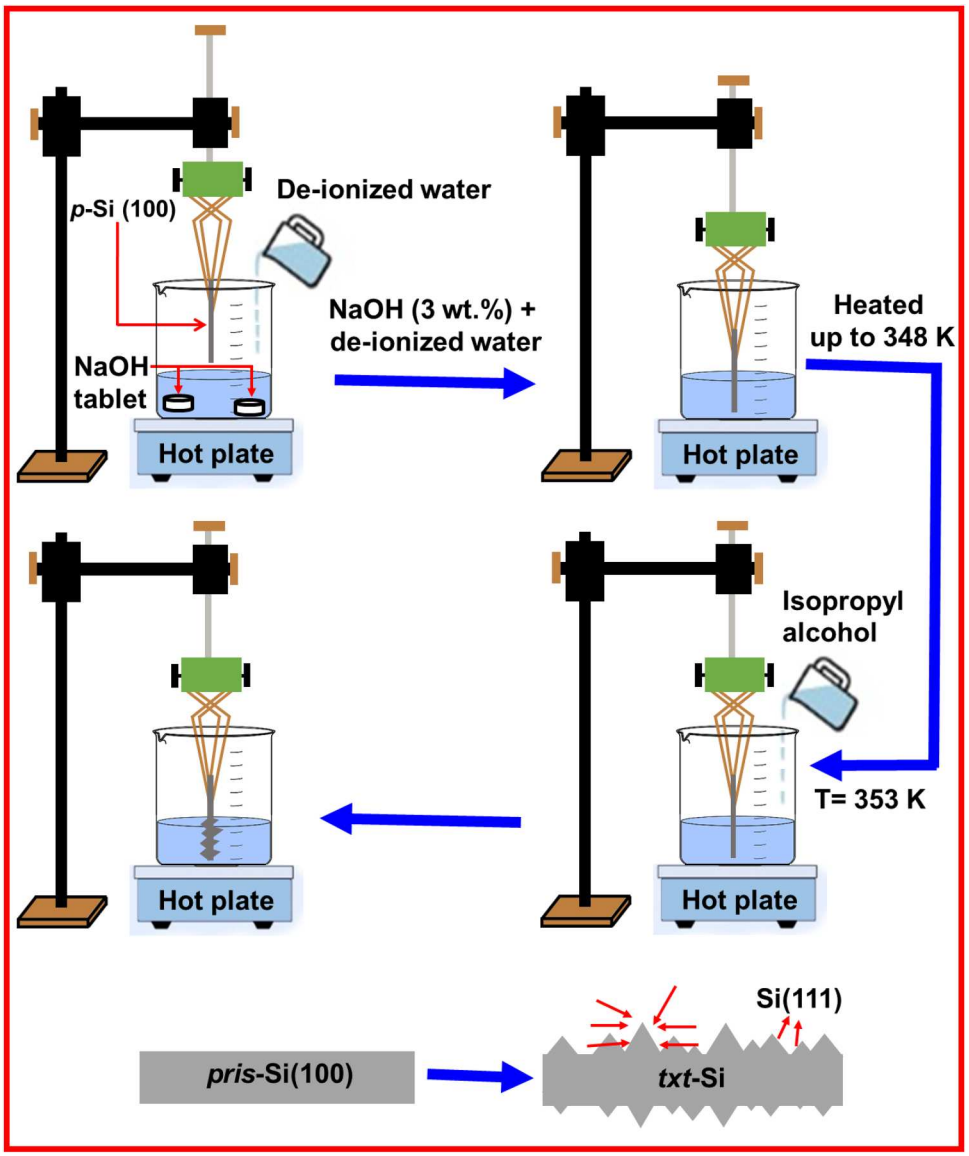


**FIG. 1.** Schematic of the experimental setup used for chemical etching of Si(100) substrates.

Carl-Zeiss, Germany) using 5 keV electrons and atomic force microscopy (AFM) (Asylum Research, MFP3D, USA), operating in the contact mode. In order to understand the underlying mechanism behind the evolution of surface morphology under alkaline etching, numerical integrations were performed using a fourth order Runge–Kutta method and the improved spatial discretization introduced by Lam and Shin[32] for the nonlinear terms. In doing so, periodic boundary conditions were used along with lattice constant, $\Delta x = 0.5$, and time step, $\Delta t = 0.01$. The chosen initial height values were randomly distributed between 0 and 1, whereas the standard system size ($L$) of our simulations was 512. To scale the simulated images with physical dimensions, we have used the 512 pixel size of the initial surface as 10 $\mu$m. On an *ad hoc* basis, we have considered the number of iterations multiplied by time step as the effective time and compared it with the experimental etching time. The specular reflectance of the samples before and after chemical etching was measured by an ultraviolet–visible–near infrared (UV–Vis–NIR) spectrophotometer (Shimadzu 3101PC, Japan) using an unpolarized light. Field emission (FE) measurements were carried out at room temperature (RT) using a diode

configuration in a high vacuum chamber (Excel Instruments, India), under a pressure of $3 \times 10^{-7}$ mbar, which is equipped with a high voltage source meter (Keithley, 2410, USA). A vacuum compatible microgauge was employed with an anode plate to maintain a precise separation between the emitter surface and the anode. A copper block with a tip diameter of 2.5 mm (area $\approx 5 \times 10^{-4}$ mm$^2$) was used as the anode, while the etched Si (hereinafter called as *txt*-Si) substrates were used as the cathode (for FE measurements). Field emission experiments were performed by applying a bias voltage between the *txt*-Si cathode and the Cu anode plate which was positioned perpendicular to the cathode plane. AFM image analysis was carried out using the SPIP[33] and WSxM softwares.[34]

## III. RESULTS AND DISCUSSION

### A. Morphological evolution dynamics: Experiment and simulation

To investigate the temporal evolution of Si surface morphology due to chemical etching, scanning electron microscopy (SEM) and AFM measurements are performed on all samples before and after etching. Figures 2(a)–2(f) show plan-view SEM images of the microstructural evolution of the Si surface corresponding to different etching times in the range of 30–2400 s. These images depict the complete coverage of the respective surface with randomly distributed pyramids having different dimensions which increase with etching time. The surface coverage of these

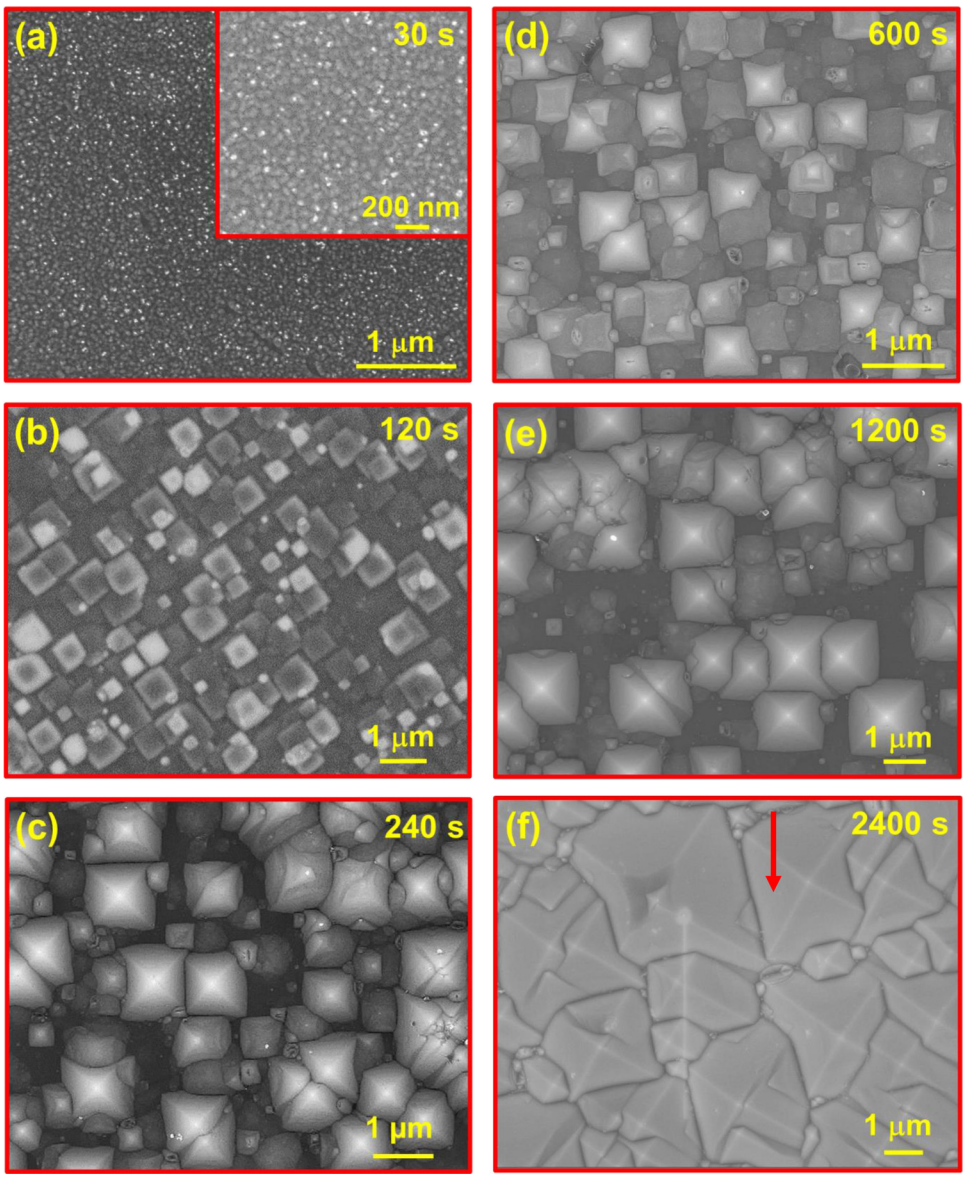


**FIG. 2.** SEM images corresponding to different etching times: (a) 30 s, (b) 120 s, (c) 240 s, (d) 600 s, (e) 1200 s, and (f) 2400 s.

pyramids ranges from 27.6 ± 2% to 85.2 ± 4% corresponding to the etching times of 60–2400 s, as shown in Table I. From Fig. 2, it becomes evident that upon increasing the etching time the surface coverage increases since at higher etching times pyramids of bigger dimensions are formed. The dimension of these pyramids ranges from 0.2 to 2 $\mu$m (for etching times in the range of 60–2400 s), as is measured from AFM images. Figures 3(a)–3(l) show the AFM topographic and respective deflection images corresponding to the morphological evolution of the Si surface subject to different etching times. The deflection images clearly show the pyramidal edges similar to the SEM images. In fact, the etching time-dependent evolution of the average size of pyramidal features is extracted from these images. It is interesting to note that for the lowest etching time (viz., 30 s), pyramid-like structures are not evident and dimensions of the evolved structures are quite small. The shape of the pyramidal structures becomes prominent with increasing etching time and starts becoming sharper as well. For etching times of 1200, 1800, and 2400 s, these pyramids form homogeneous surfaces and the highest surface coverage area is obtained for the ones who evolve corresponding to the highest etching time.

Figures 4(a)–4(c) show the line profiles obtained from the morphological images shown in Figs. 3(a)–3(f) (marked by green lines) corresponding to different etching times. For etching times up to 600 s, pyramidal structures are visible but their coverage area is low (Figs. 2 and 3). On the other hand, for etching times >600 s, bigger pyramidal structures appear having a wide distribution in size. For solar cell applications, maximum absorption of light is desirable for which the aspect ratio ($d/a$) of the pyramidal structures should be 2–2.5 $\mu$m, and hence, an attempt has been made in this work to achieve the same. Figure 4(d) shows variations in the aspect ratio and average facet angle of the pyramidal structures with etching time. This reveals a rapid decrease in the aspect ratio of pyramidal structures (up to 600 s) which gets saturated (2 $\mu$m) at higher etching times, whereas an opposite trend is observed for the average facet angle of pyramidal structures [i.e., it increases rapidly up to an etching time of 600 s and shows a saturation (~45°) beyond the same].

The overall etching reaction in NaOH solution may be expressed as follows:[22]

$$Si + 2H_2O + 2OH^- \rightarrow Si(OH)_4 + 2H_2. \quad (1)$$

Such a reaction proceeds at a lower rate in the absence of any one of the reactants $H_2O$ and $OH^-$. In this reaction, produced $H_2$ is seen as bubbles which escape from the reaction vessel. These bubbles work as masks by creating temporary localized etch steps by sticking on the substrate.[22] However, etching rate is a function of crystalline orientation, doping, and the etchant composition.[22] In the present case, surface roughening in the form of hillock formation is observed and the resulting morphology is governed by the anisotropic etching that produces randomly distributed pyramids. As a matter of fact, for the formation of pyramids, lateral etching of the surface is very important which is achieved by the help of hydrogen bubbles formed during the etching process. Singh *et al.* have shown that during the etching of a *c*-Si substrate, the etching rate of the {111} surface is lower compared to the {100} or {110} surface and the ratio of the etching rate for {100} to {111} surfaces is ~35.[9] The lower etching rate of the {111} plane is due to its higher activation energy in comparison to the {100} plane.[25,35] Therefore, the pyramid formation takes place along the {111} plane, as is shown by an arrow in Fig. 2(f). For the lowest etching time (i.e., 30 s), the spacing between two adjacent pyramids is difficult to separate out from the corresponding SEM image, although the AFM phase image [Fig. 3(d)] clearly manifests the nucleation of pyramidal structures on the Si surface.

Several theoretical explanations have been put forward to explain the formation of pyramids/hillocks on *c*-Si surfaces.[28,36] However, macroscopically any morphological instability can be understood in light of stress-induced roughening phenomenon.[36] Based on the Marangoni effect, when two fluids are in contact, there is an interfacial tension gradient at the surface which works as the driving force for fluid transport.[37,38]

Here, we will consider that atoms are removed only by chemical reaction during etching. This results in a current flow from the surface, and this process obeys a continuity equation in the form of their height, $h$. The evolution of a surface height $h(x,t)$ can be described in a coarse-grain approach by a partial differential equation[39]

$$\frac{\partial h}{\partial t} = -\nabla \cdot \vec{j}, \quad (2)$$

**TABLE I.** Extracted relevant parameters from pyramidal *txt*-Si surfaces fabricated under different etching times.

| Etching time (s) | RMS roughness (nm) | Skewness | Kurtosis | Aspect ratio ($d/a$) | Coverage area (%) | Average facet angle (deg) | $R$% (at 550 nm) | $E_{to}$ (V $\mu$m$^{-1}$) | $\beta$ |
|---|---|---|---|---|---|---|---|---|---|
| 30 | 11.34 | 0.12 | 7.62 | … | 73.26 ± 2 | … | 42 | 30.01 | 127.6 |
| 60 | 35.65 | 0.12 | 6.51 | 4.34 ± 0.28 | 27.57 ± 1 | 25.66 ± 4.3 | 37.27 | 27.42 | 204.6 |
| 120 | 46.70 | 0.13 | 4.84 | 3.17 ± 0.25 | 38.12 ± 4 | 26.73 ± 3.5 | 21.69 | 23.14 | 275 |
| 240 | 101.17 | 0.13 | 3.36 | 2.88 ± 0.21 | 42.50 ± 1 | 33.28 ± 3.9 | 2.7 | 18.13 | 485.29 |
| 360 | 148.42 | 0.14 | 2.84 | 2.80 ± 0.25 | 49.19 ± 5 | 35.72 ± 3.1 | 0.70 | 13.06 | 502.3 |
| 480 | 165.68 | 0.24 | 2.81 | 2.29 ± 0.23 | 53.78 ± 2 | 40.12 ± 2.8 | 0.53 | 8.11 | 1238.3 |
| 600 | 198.20 | 0.26 | 2.64 | 2.44 ± 0.19 | 58.70 ± 6 | 41.92 ± 3.6 | 0.39 | 4.62 | 1632.4 |
| 1200 | 279.22 | 0.29 | 2.59 | 2.51 ± 0.20 | 63.90 ± 4 | 43.23 ± 1.9 | 0.34 | 2.62 | 3591.2 |
| 1800 | 285.43 | 0.31 | 2.58 | 2.35 ± 0.17 | 76.33 ± 3 | 42.9 ± 1.6 | 0.30 | … | … |
| 2400 | 294.51 | 0.32 | 2.54 | 2.37 ± 0.14 | 85.19 ± 4 | 44.19 ± 1.4 | 0.25 | … | … |

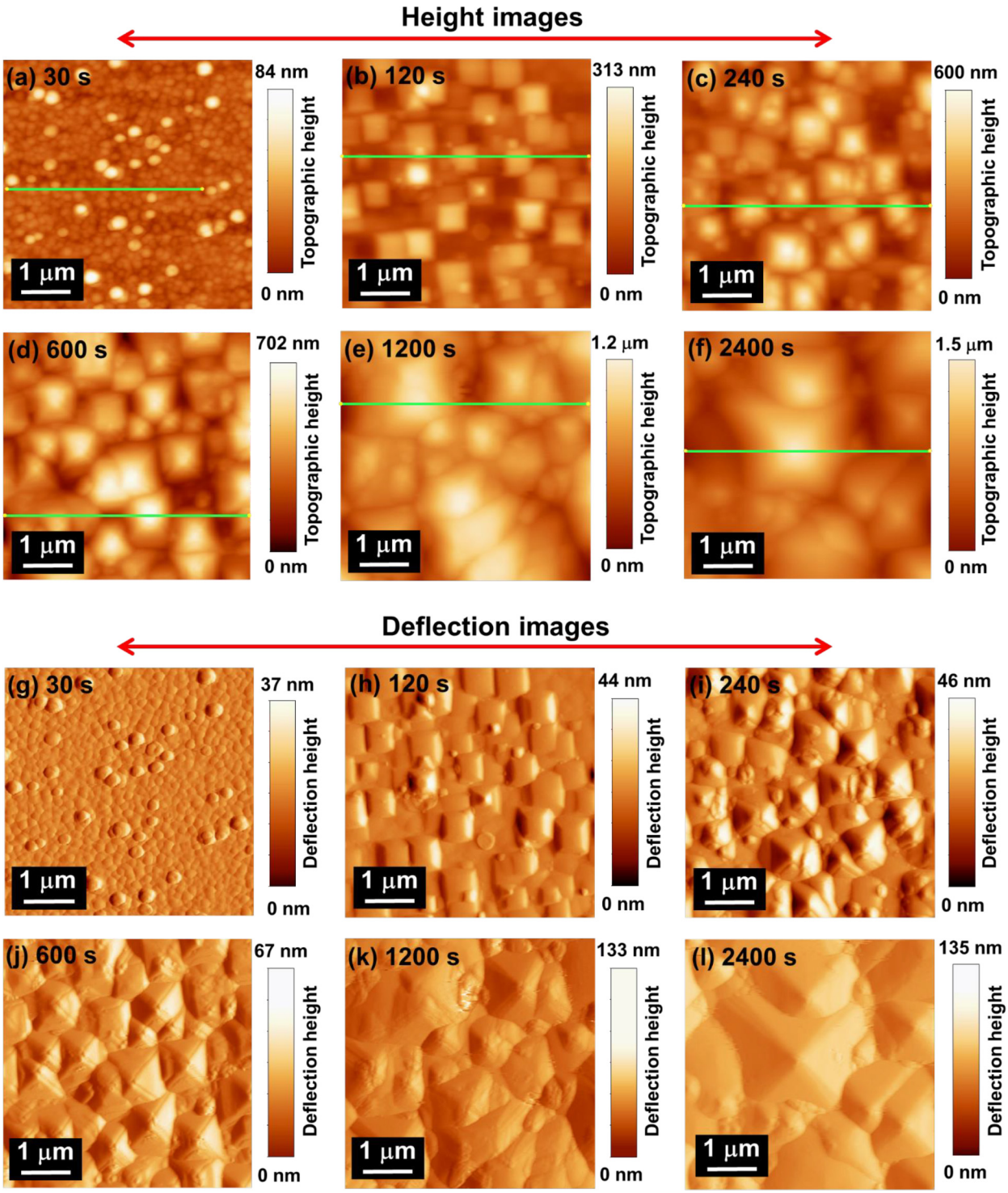


**FIG. 3.** Contact mode AFM images of IPA-etched Si surfaces corresponding to different etching times. Topography images: (a) 30 s, (b) 120 s, (c) 240 s, (d) 600 s, (e) 1200 s, and (f) 2400 s and corresponding deflection images (deflection images collected during the topography measurements): (g) 30 s, (h) 120 s, (i) 240 s, (j) 600 s, (k) 1200 s, and (l) 2400 s. The deflection images show the clear edges of pyramids. All image sizes are of $5 \times 5\,\mu m^2$.

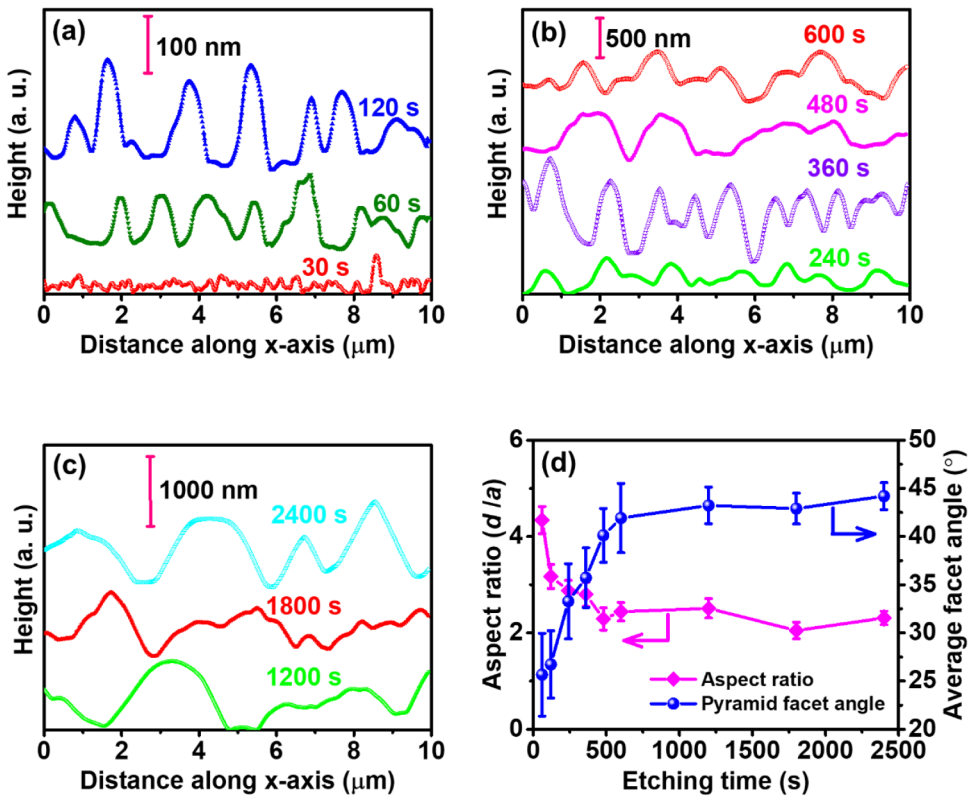


**FIG. 4.** (a)–(c) Line profiles obtained from pyramidal structures corresponding to different etching times. (d) The plot of an aspect ratio and an average facet angle as a function of etching time of *txt*-Si samples.

where $\vec{j}$ is a bulk rate of mass flow. The continuity equation follows the conservation law. In general, $\vec{j}$ is given by the gradient of a chemical potential, $\mu$. During the etching process, surface atoms gain an activation energy and are removed from the surface just after coming in touch with the etchants. The other important model for interface growth is the Kardar–Parisi–Zhang (KPZ) model[40]

$$\frac{\partial h}{\partial t} = R_d - \nu\nabla^2 h + \sigma(\nabla h)^2 + \eta, \tag{3}$$

where $R_d$ is the growth rate and $\nu\nabla^2 h$ is the surface tension term as it tends to smoothen the interface. The nonlinear term, $\sigma(\nabla h)^2$, accounts for growth along the normal direction (lateral growth). However, this description can be applied only to uncorrelated noisy systems. Subsequently, Kessler *et al.* proposed modifications in the KPZ model which is known as the Kessler-Levine-Lu (KLT) model.[29]

According to this model, a fluid moves at the interface through a random medium which can be described as

$$\frac{\partial h}{\partial t} = F + \nu\nabla^2 h + \eta(x, t), \tag{4}$$

where $F$ is the pushing (piston driving) force applied in order to compress the fluid and $\eta(x, t)$ represents the quenched noise. This model is typically used for percolation processes. Thus, to apply the KLT model on corrosion processes, the piston driving force $F$ is associated with the etching rate and the quenched noise $\eta(x, t)$ is represented by the silicate mask. According to this model, the number of etchant ions in the liquid decreases when the etching time increases and as a consequence, the etching power also decreases. Here, this pushing force generates a stress at the interface of the etchant and the substrate. This stress-induced roughening leads to a variation in the surface configuration. In fact, during chemical etching, direct addition and removal of atoms occur from a surface. However, the alkaline etching of Si depends on the orientation of a plane. This orientation-dependent alkaline etching indicates a specific spatial symmetry in the system. As the same crystalline substrate does not show any pyramidal structures in acidic etchants,[41] we have concluded that this symmetry is a combined effect of both the substrate and the etchant solution.

For a Si(100) substrate, etching always takes place in the ⟨100⟩ direction, whereas under a similar etching condition, there is no pyramid formation for a Si(111) substrate. Thus, in order to describe the formation of pyramidal structures on Si with their spatial symmetry, we can generalize the continuum equation [Eq. (3)] by using a potential barrier, $U(m_x, m_y)$, because the removal of surface atoms

behaves like a current flow which is controlled by the specific potential barrier. This potential barrier must be a function of the local slopes, $m_i = \frac{\partial h}{\partial i}$ $(i = x, y)$, of a surface. The current flow $(\vec{j}_F)$ in the form of the removal of atoms from the surface can be related to the surface height by the law of mass conservation, as described in Eq. (1). Thus, the current produced by the potential barrier controls the removal of atoms during the etching process and is related to the potential by $\vec{j}_F = \frac{\partial U}{\partial m}$. Here, we have considered a fourfold symmetric potential—which is a polynomial function of local slopes $(m)$ along $x$- and $y$-directions—given by

$$U = am_x^4 + bm_x^2 + bm_y^2 + am_y^4, \tag{5}$$

where the parameters $a$ and $b$ are constants and are chosen in such a way that a proper barrier potential is generated. Using this potential in a MATLAB™ program (version 7.14), we integrate the following continuum equation:

$$\frac{\partial h}{\partial t} = -\nabla \vec{J}_F + \sigma(\nabla h)^2 + \eta. \tag{6}$$

Figure 5(a) shows the fourfold symmetric potential corresponding to $a = 1$ and $b = -1$ and is used to reproduce the experimentally observed pyramidal structures. The $x$- and $y$-axes in the plot of potential represent the local slopes $(m_x, m_y)$ along $x$- and $y$-directions, while the $z$-axis represents the potential as discussed above.[42] Figures 5(b)–5(f) show the simluated images of etched Si surfaces using Eqs. (5) and (6). In fact, Fig. 5(b) shows that for a lower number of iterations, pyramidal structures nucleate on the surface in a random manner. However, as the number of iterations increases, a large number of pyramids appear on the surface and the separation between two consecutive pyramids starts decreasing which matches very well with our experimental observations (Fig. 3). On the other hand, Figs. 5(e) and 5(f) show closely packed pyramidal structures having sharper features and their dimensions get almost saturated. To compare the experimentally observed temperal evolution of etched Si surface morphology with the simulated results, we have extracted various statistical parameters. Among the height amplitude, parameters such as roughness, skewness, and kurtosis present the global average quantities which help in understanding the behavior of a surface as a whole. The roughness, skewness, and kurtosis values corresponding to different etched times are presented in Table I. The positive skewness values obtained from the etched surfaces indicate surfaces with more peaks in the pyramids, whereas the kurtosis describes the sharpness of the pyramidal structures. We get positive skewness for all etching times and at early etching time, (up to an etching time of 60 s) kurtosis indicates a sharp height distribution profile. With increasing etching time, the sharp apex of pyramidal structures also gets etched to form blunt pyramidal peaks. To find the correlation of the height at two distant points, we have calculated the power spectral density (PSD) and autocorrelation function of the *textured*-Si surfaces. Figure 6 shows the PSD and height–height correlation curves obtained from the AFM images (Fig. 3) and simulated surfaces (Fig. 4). Figures 6(a) and 6(b) show the radially averaged PSD depending on the wave vectors. The behavior of the PSD curves shows a $k$-independent feature at small wave vectors, indicating an uncorrelated behavior at large distances. The power law decay of PSD can be expressed as $S(k) \sim 1/k^{2\alpha+2}$ with the roughness exponent $\alpha$ that are correlated.[24] Figure 6(a) shows a crossover region from the correlated to uncorrelated region which changes with etching time as the correlation length increases. The points that separate the correlated $k$ with the uncorrelated one determine the correlation length. For an etching time of 30 s, we find that the correlation length is 100 nm which increases to 1000 nm for an etching time of 120 s and after which saturation occurs. On the other hand, the PSD curves overlap with each other, confirming the fact that the pyramids are almost isotropic. The same behavior is obtained from the height–height correlation function shown in Figs. 6(c) and 6(d) for experimental and simulated surfaces, respectively. The measured exponents $(\alpha)$ from the PSD curves as well as from the height–height correlation at early stages of etching are found to be <0.5, indicating a kinetically rough or self-affined surface which exceeds the value 1 at higher etching times. The comparison of the simulated surface with the experimentally observed surface sheds some light on the morphological evolution by chemical reaction using a physical generic equation.

In the present case, it is observed from the experimental SEM images that the height and dimension of pyramids are of the order of 1–2 $\mu$m which fulfills the criteria to achieve a significant reduction in the surface reflectance (as is discussed earlier). In order to verify the same, we have carried out systematic reflectance measurements on *txt*-Si substrates, fabricated under different etching times, which is described below.

### B. Optical and field emission properties

Figure 7(a) shows the specular reflectance data of textured-Si samples formed under different etching times (in the wavelength range of 300–3000 nm) and is compared to that obtained from pristine-Si (unetched sample). It is observed from Fig. 7(a) that with increasing etching time, the average specular reflectance shows a decreasing trend. The surface reflectance of pristine-Si (which hereinafter will be called as *pris*-Si) is ~43.5%, whereas in the case of lower etching times, viz., for 30 and 60 s, it reduces to 42% and 37.27%, respectively (at 550 nm).[9,28] Thus, the observed change in the surface reflectance is minimal for lower etching times which can be attributed to less well-defined structures on Si surfaces. However, corresponding to an etching time of 120 s, there is a substantial drop in the surface reflectance (≈20%) which keeps reducing in a systematic manner with an increase in the etching time. It further reduces to 0.5% for an etching time of 600 s. Higher etching times up to 2400 s causes even lower (≈0.25%) reflectance value over the broad wavelength range of 300–3000 nm. For a better clarity, a magnified part of Fig. 7(a), in the wavelength range of 300–800 nm, is shown in Fig. 7(b), which depicts the reflectance data for etching times of 240–2400 s. It becomes evident that the reflectance value drops drastically to 3% for an etching time of 240 s, which further reduces close to 0.25% for the longest etching time, i.e., 2400 s.

Recently, Imamura *et al.* have shown the effect of refractive index on the reflectance of a nanocrystalline-Si layer on pyramidally textured-Si surfaces, grown by acidic etching, and achieved a minimum reflectance in the range of 0.96% and 3.76% (in the wavelength range of 300–800 nm).[43] Likewise, Jiang *et al.*[23] and

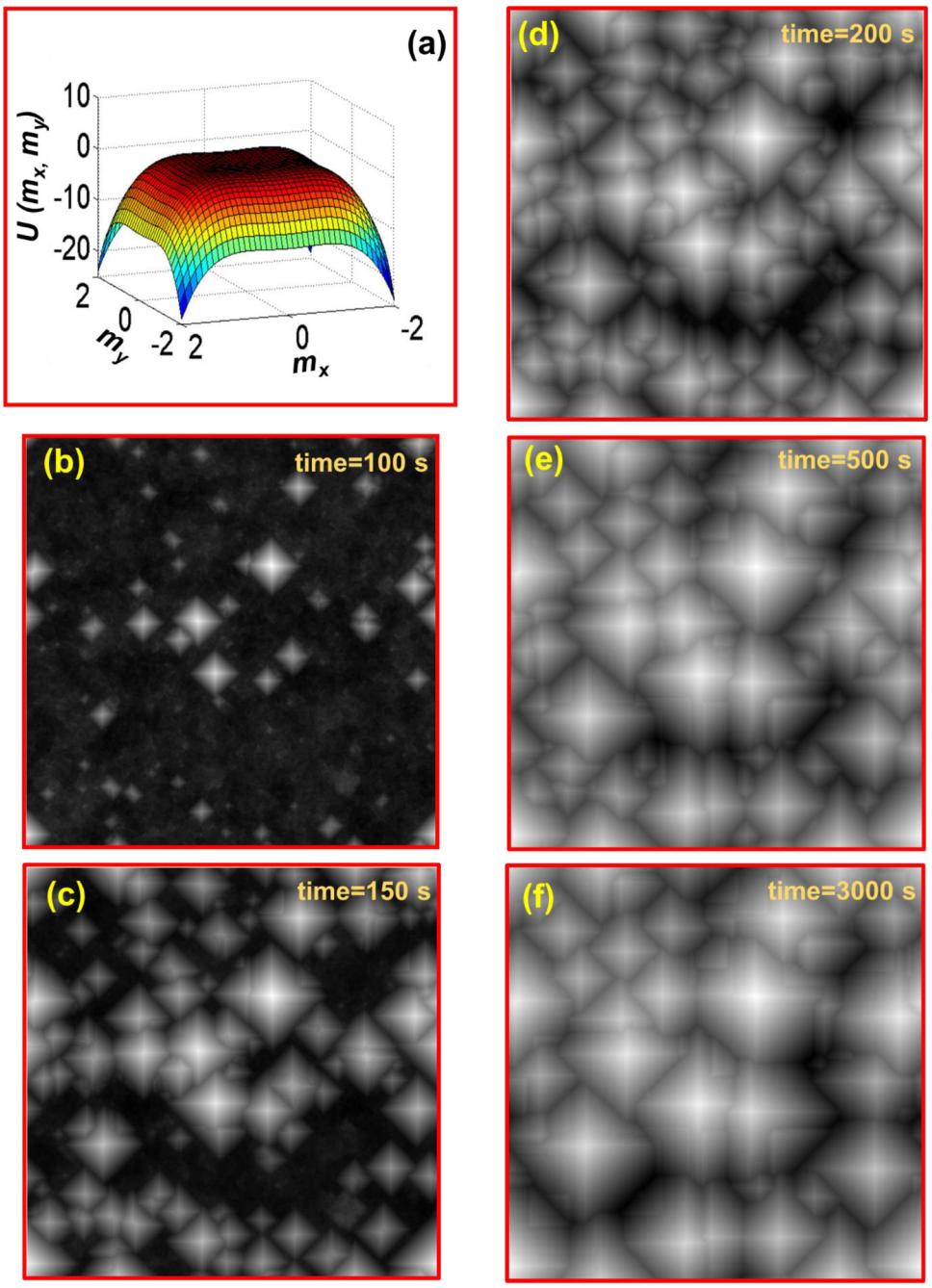


**FIG. 5.** (a) The anisotropic potential barrier as a function of local slopes ($m_x$ and $m_y$) that governs the etching process. (b)–(f) Evolution of the simulated surface for different iteration times ($t$): (b) 100 s, (c) 150 s, (d) 200 s, (e) 500 s, and (f) 3000 s.

Otto *et al.*[44] have shown low average reflectance for black-Si in the range of 2.4%–4.7%. In another report, average optical reflectance of slantingly and vertically aligned silicon nanowire arrays has shown about 5% and 2.5% over the wavelength range of 300–1000 nm, respectively.[3] Thus, it is interesting to note that this hitherto unseen low optical reflectance exhibited by Si pyramids sets a benchmark than the ones achieved by more sophisticated texturing approaches.[23,44,45] This reduction in the surface reflectance can be understood from the schematic optical ray diagram, as is shown in Fig. 7(c) where a pyramidally textured-Si surface leads to light trapping due to multiple reflections of light from the pyramids.[16] When light is incident on the top region of the pyramidal surfaces, due to low incident angle, it has the highest probability of reflection. On the other hand, light

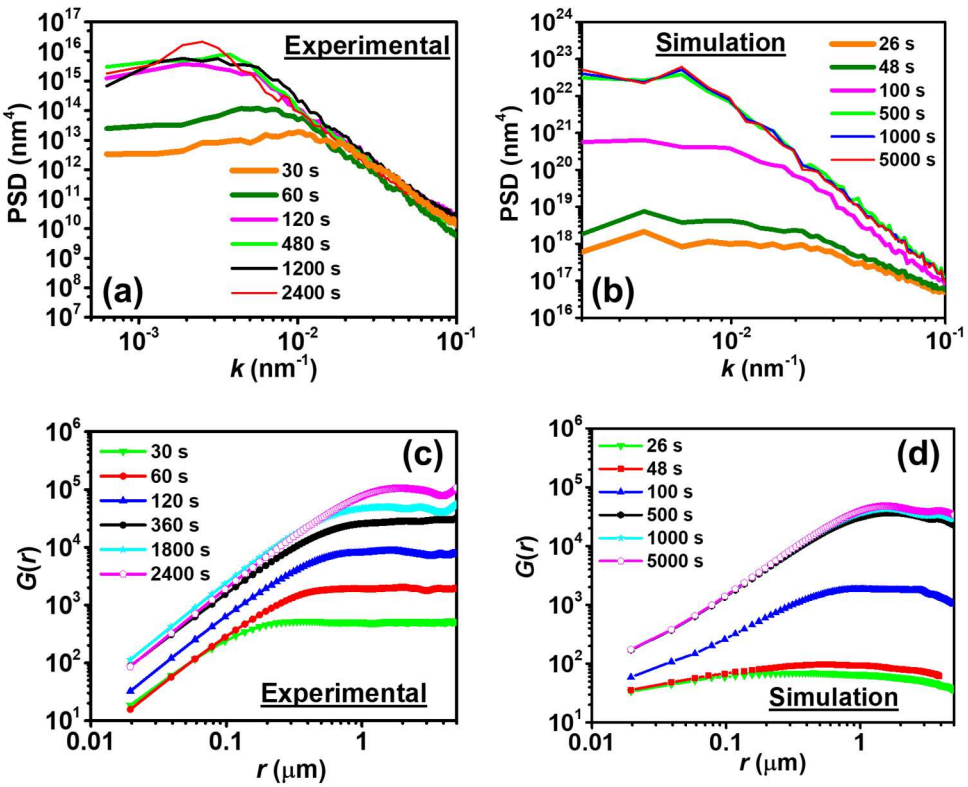


**FIG. 6.** (a) and (b) Log–log plot of the (radially averaged) PSD curves of experimental and simulation studies for different times, respectively. (c) and (d) Height–height correlation functions vs lateral distance obtained for *textured* surfaces of different etched times.

incident on the bottom region of pyramids undergoes multiple reflection and reduces the surface reflection.[9] Likewise, each pyramid helps to reflect the incident light and let it incident on an adjacent pyramid. Consequently, reflectance from the front surface decreases from 43.5% to 0.25%. In addition, the low reflectance of *txt*-Si surfaces formed at higher etching times is due to highly dense and randomly distributed pyramids having facet angles close to 45°, as confirmed from the corresponding SEM and AFM images.[16] It is interesting to note that during the early etching period, the surface of silicon just starts to get roughened and at this stage dimensions of the evolved structures are quite small to trap light in an efficient manner. In fact, it is known that the reflectance is strongly influenced by the size of the pyramids and light having higher wavelengths than the size of pyramidal structures cannot undergo multiple reflections.[9,46] Sai *et al.* have shown the effect of pyramid dimension on antireflection and light trapping properties of textured-Si surfaces using a numerical simulation based on Maxwell's equation.[46] They have observed that surface reflection loss can be reduced significantly by using submicron Si surfaces. On the other hand, a similar trend in size of pyramids and reflectance (lowest value of reflectance is ∼11% in the visible region) was observed experimentally by Singh *et al.* from *textured*-Si surfaces which are prepared in aqueous alkaline solutions.[9] In addition to Si, there are other studies on texturing of semiconductors, such as Ge,[47] InP,[48] GaAs,[49] etc., and their further use in the photovoltaics to enhance the photovoltaic cell efficiency. As a matter of fact, the reflectance of such textured surfaces changes significantly due to the size of pyramids, affecting the overall refractive index of the samples to a large extent. Thus, based on the above results, it can be inferred that pyramidally textured-Si surfaces, having the right kind of aspect ratios, can give rise to efficient and tunable light trapping.

In order to explore multiple functional properties of such pyramidally textured surfaces, having reasonably sharp apexes, field emission studies are carried out on the same. Si microstructures having sharp apexes/tips have been shown to exhibit field emission property with reasonably low turn-on fields as electron tunnelling is strongly influenced by the physical and geometrical properties of a material.[50,51] Field emission-based devices have numerous potential applications in flat panel displays, microwave power amplifiers, etc.[52,53] In the field emission process, electrons emit from the cathode and strike the anode due to an applied electric field which can modulate the height of the potential barrier at the emitter surface–vacuum interface.[54] This phenomenon is explained on the basis of the Fowler–Nordheim (F–N) model.[55] According to this model, electrons are emitted from a

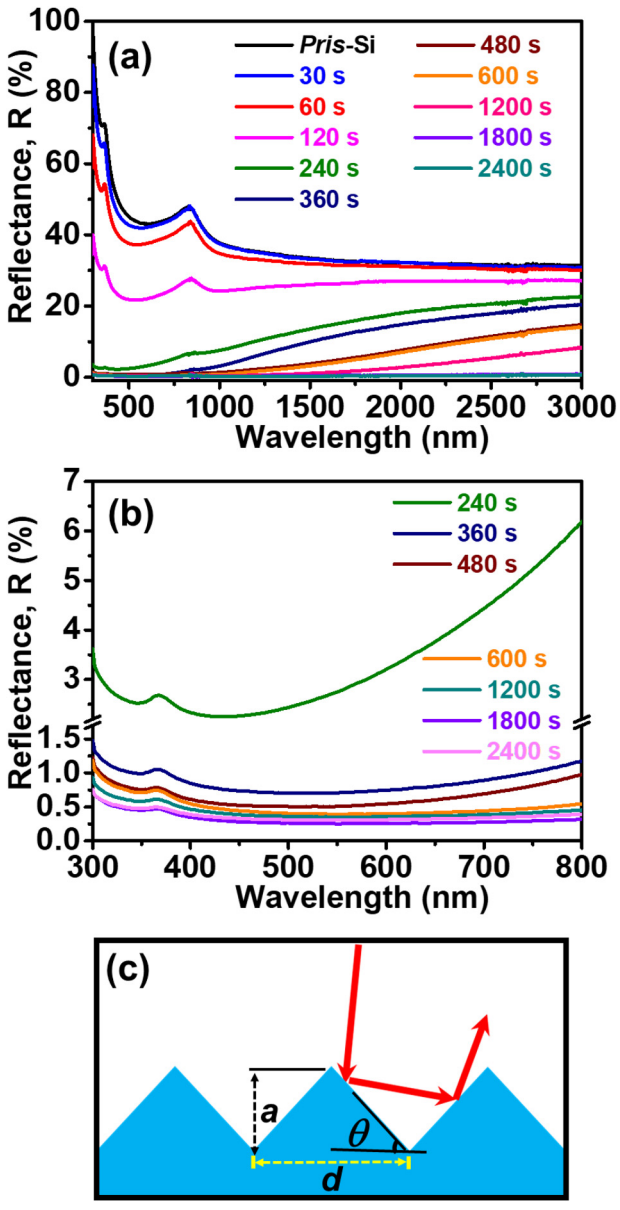


**FIG. 7.** (a) and (b) The reflectance ($R$%) spectra of chemically prepared pyramidally textured-Si substrates for different etching times in the wavelength range of 300–3000 nm and 300–800 nm, respectively. (c) The schematic diagram showing optical reflection from a pyramidally textured-Si surface. The pyramids shown here can be considered as a schematic cross-sectional view of the pyramidal structures presented in Fig. 3, and the experimental topographic height of those pyramids can be correlated with the average height shown in the schematic.

semiconductor due to the quantum tunnelling effect. The famous F–N equation can be expressed as[55]

$$J = \frac{A\beta^2 E^2}{\phi} \exp\left(-B\phi^{\frac{3}{2}}/\beta E\right), \tag{7}$$

where $J$ is the emission current density ($\mu$A cm$^{-2}$), $A$ and $B$ are constants with $A = 1.56 \times 10^{-10}$ A V$^{-2}$ eV and $B = 6.63 \times 10^3$ V $\mu$m$^{-1}$ eV$^{-3/2}$, $E$ is the mean electric field between the electrodes (V $\mu$m$^{-1}$), $\beta$ is the field enhancement factor (depends on the tip-sample geometry), and $\phi$ is the work function (eV) of the emitter.

The field emission from the emitter surface toward the metallic anode is achieved by studying $J$–$E$ (current density–applied electric field) characteristics under an applied electric field. Figures 8(a) and 8(b) show the field emission properties (current density vs applied electric field) of *txt*-Si substrates, prepared under alkaline etching, for different etching times of 30–360 s and 480–1200 s, respectively. It becomes evident that the highest turn-on field ($E_{to}$) of 30.01 V $\mu$m$^{-1}$ is observed for a Si sample etched for 30 s [Fig. 8(a)] whereas the lowest $E_{to}$ of 2.62 V $\mu$m$^{-1}$ is manifested by the sample prepared under an etching time of 1200 s [Fig. 8(b)]. For intermediate etching times of 60, 120, 240, 360, 480, and 600 s, $E_{to}$ values turn out to be 27.42, 23.14, 18.13, 13.06, 8.11, and 4.62 V $\mu$m$^{-1}$, respectively. It is interesting to note that the observed $E_{to}$ value for cold cathode emission from the *txt*-Si substrate prepared for an etching time of 600 s is lower than that of Si nanotube arrays ($E_{to}$ = ~5.1 V $\mu$m$^{-1}$).[56,57]

Figures 8(c) and 8(d) show $1/E^2$ vs $\ln(J/E^2)$ plots for different etching times in the range of 30–360 s and 480–1200 s, respectively, which are fitted linearly, confirming that the F–N tunneling process is operative for the present study.[56] Interestingly, the F–N tunneling from *txt*-Si substrates shows different slopes. It is, therefore, interpreted that in addition to F–N tunneling some other contributing factors may also be involved.[58] Electron tunneling in the high field region obeys the F–N tunneling. By using the slope of F–N plots [Figs. 8(c) and 8(d)], enhancement factor ($\beta$) can be calculated from the following equation:

$$\beta = -6.83 \times 10^3 (\phi)^{3/2}/\text{slope}. \tag{8}$$

The values of enhancement factor ($\beta$) for different *txt*-Si substrates are calculated from the slopes of the respective fitted lines which turn out to be 127 (for 30 s) and 3591 (for 1200 s), assuming the work function of bulk-Si (i.e., 4.8 eV).[52] To the best of our knowledge, the observed values of $E_{to}$ and $\beta$ are among the best reported ones on chemically prepared textured-Si substrates.[56] It may be mentioned that the calculated values of $\beta$ and $E_{to}$ for intermediate etching times are summarized in Table I which confirm the tunability in cold cathode electron emission from chemically prepared Si pyramids. In addition, it is interesting to note that in the present case, a decrease in the $E_{to}$ value is observed with increasing etching time, whereas an opposite trend is observed for $\beta$ values of the same pyramidal structures as seen from Fig. 8(e).

The similar trends in turn-on potential and enhancement factor are observed by Zorba *et al.* from Si-spikes which are fabricated by ultraviolet laser pulses where higher enhancement factors are obtained at lower turn-on fields.[59] In our case, it is also observed (data not shown) that the pristine-Si sample does not give rise to any field emission up to 1000 V (the present instrumental limit). Similarly, no signature of field emission is observed for etching times of 1800 and 2400 s which can be attributed to much bigger dimensions of the pyramids.[59] Recently, Basu *et al.* have shown that mostly

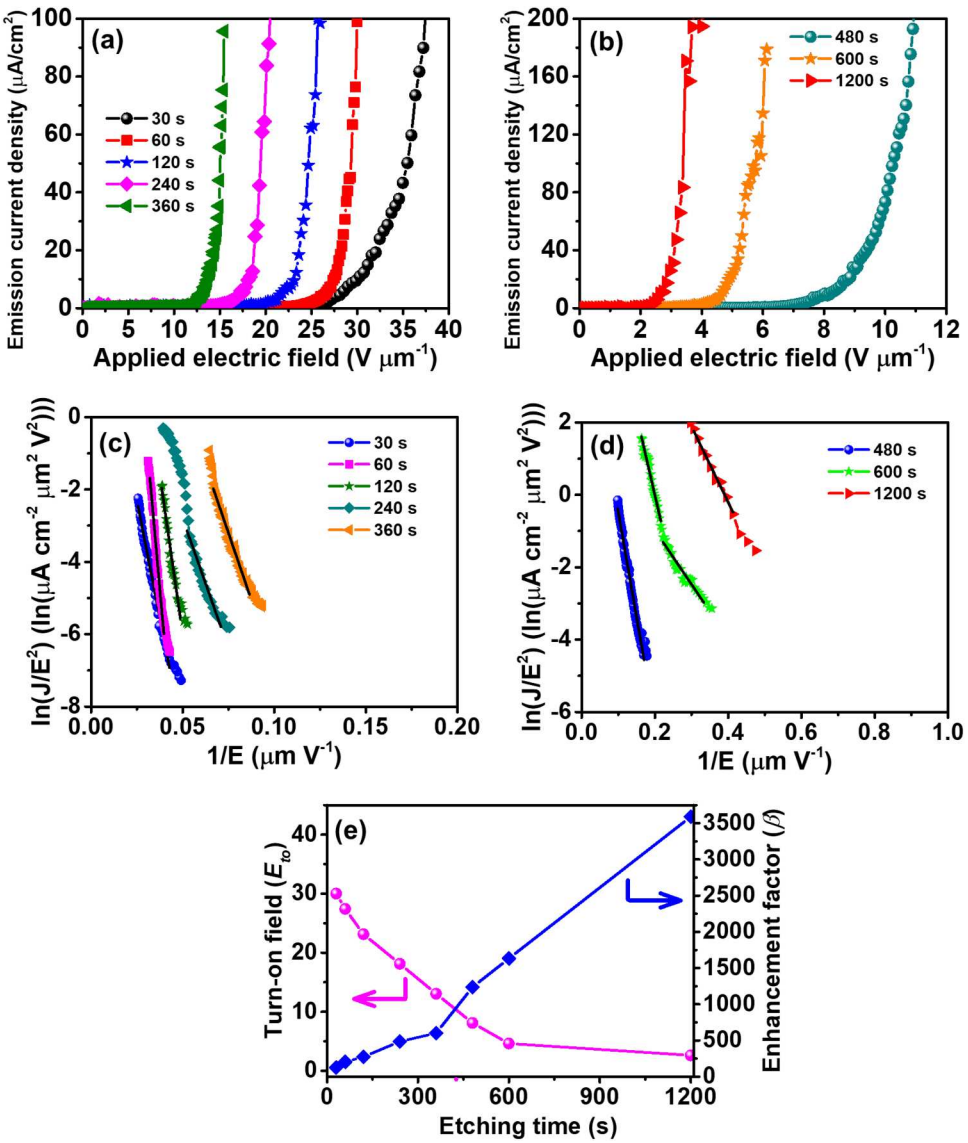


**FIG. 8.** (a) and (b) The field emission current density obatined from *txt*-Si substrates fabricated for etching time of 30–360 s and 480–1200 s, respectively, as a function of the applied electric field, *E*. (c) and (d) The F–N plots as a function of 1/*E* for *txt*-Si substrates fabricated under etching time of 30–360 s and 480–1200 s, respectively. The solid lines are the linear best fits to the data. (e) The plot of turn-on field and field enhancement factor ($\beta$) as a function of etching time of *txt*-Si samples.

the valleys and a small part of the side walls of the nanofacets of Si, rather than apexes, contribute to the electron emission process and the height of these nanofacets are of the order of 200 nm (highest one), whereas in the present case the pyramids have dimensions of the order of micrometer.[52] The efficient field emission from pyramidally textured-Si surfaces is ascribed to the enhanced aspect ratio and sharpness of the pyramids up to a certain limit.[56,60,61] In order to compare the present field emission data with other results on textured-Si and carbon nanotubes, we have chosen some recent reports.[51,54,56,60,62] For instance, Fung *et al.* have shown the field emission characteristics of chemically prepared textured-silicon surfaces where lowest turn-on potential is 9 V $\mu m^{-1}$. In addition, carbon nanotubes are known to exhibit low turn-on potential ($E_{to} = 2.70$ V $\mu m^{-1}$)[56] and thus, Chang *et al.* have shown that a carbon nanotubes/graphene composite film deposited on textured-Si shows very low turn-on potential ($E_{to} = 0.45$ V $\mu m^{-1}$).[62] In the present case, we observe that the lowest $E_{to}$ is 2.62 V $\mu m^{-1}$ which is lower than the abovementioned value only for textured-Si surfaces and close to a carbon nanotube-based system. We need to keep in mind that stability of *txt*-Si surfaces is always a concern

compared to carbon nanotubes. However, a very easy and cheap fabrication process of these textured surfaces by alkaline etching, exhibiting etching time-dependent tunable field emission (from 3 to 30 V $\mu m^{-1}$), makes it a promising route for use as short-lived filaments, e.g., protective safety devices.

## IV. CONCLUSIONS

In summary, we demonstrate the temporal evolution of chemically etched silicon surfaces and carry out corresponding simulation studies using a continuum theory based on stress-induced morphological instability. Field emission gun-based scanning electron microscopy and atomic force microscopy show the time evolution of chemically prepared pyramidal structures having a random distribution. It is observed that initially with increasing etching time, dimensions of the pyramidal structures increase rapidly, but for longer etching times, the same get saturated. In addition, using a numerical simulation based on a continuum equation, it is shown that similar pyramidal features can be reproduced. Simulation study on the evolution of morphology during chemical etching, using a generic equation, is an attempt toward a generalized understanding of a chemical reaction from a physical perspective. However, further study is required to generalize the equation to have a better understanding on the evolution of etched morphology of other semiconductors using different reactants. We have compared the statistical surface parameters obtained from experimental results with the simulated ones. It is also shown that chemically etched *txt*-Si substrates can be used as a very efficient absorber of light over the broad wavelength range (300–3000 nm). Further to this, the pyramidal structures exhibit an impressive tunability in the turn-on field and enhancement factor. The observed field emission in the *txt*-Si substrate confirms the Fowler–Nordheim tunneling process. The present study paves the way for designing low turn-on potential field emitting devices and/or a wide range of photoabsorption-based energy harvesting devices.

## ACKNOWLEDGMENTS

R.S. acknowledges Homi Bhabha National Institute (HBNI) and Department of Atomic Energy (DAE) of the Govt. of India, Mumbai, for providing financial assistance. S.A.M. thanks Science and Engineering Research Board (SERB), Department of Science and Technology (DST), India, for the partial financial support through a National Postdoctoral Fellowship (File No. PDF/2016/001653/PMS).

## REFERENCES

[1]V. Schmidt, H. Riel, S. Senz, S. Karg, W. Riess, and U. Gösele, Small **2**, 85 (2006).
[2]B. Tian, X. Zheng, T. J. Kempa, Y. Fang, N. Yu, G. Yu, J. Huang, and C. M. Lieber, Nature **449**, 885 (2007).
[3]H. Fang, X. Li, S. Song, Y. Xu, and J. Zhu, Nanotechnology **19**, 255703 (2008).
[4]C. K. Chan, H. Peng, G. Liu, K. McIlwrath, X. F. Zhang, R. A. Huggins, and Y. Cui, Nat. Nanotechnol. **3**, 31 (2008).
[5]F. Patolsky, G. Zheng, and C. M. Lieber, Nat. Protocol **1**, 1711 (2006).
[6]J. Oh, H. C. Yuan, and H. M. Branz, Nat. Nanotechnol. **166**, 743 (2012).
[7]M. Kumar, B. Satpati, A. Singh, and T. Som, Solar RRL, **7** 1700216 (2018).
[8]A. Mavrokefalos, S. E. Han, S. Yerci, M. S. Branham, and G. Chen, Nano Lett. **12**, 2792 (2012).
[9]P. K. Singh, R. Kumar, M. Lal, S. N. Singh, and B. K. Das, Sol. Energy Mater. Sol. Cells **70**, 103 (2001).
[10]T. H. Her, R. J. Finlay, C. Wu, S. Deliwala, and E. Mazur, Appl. Phys. Lett. **73**, 1673 (1998).
[11]M. Moreno, D. Daineka, and P. Roca i Cabarrocas, Sol. Energy Mater. Sol. Cells **94**, 733 (2010).
[12]E. Garnett and P. Yang, Nano Lett. **10**, 1082 (2010).
[13]T. Basu, J. R. Mohanty, and T. Som, Appl. Surf. Sci. **258**, 9944 (2012).
[14]M. Engler, S. Macko, F. Frost, and T. Michely, Phys. Rev. B **89**, 1 (2014).
[15]Z. Huang, N. Geyer, P. Werner, J. De Boor, and U. Gösele, Adv. Mater. **23**, 285 (2011).
[16]C. P. Saini, A. Barman, M. Kumar, P. K. Sahoo, T. Som, and A. Kanjilal, Appl. Phys. Lett. **105**, 123901 (2014).
[17]R. Singh, M. Kumar, M. Saini, A. Singh, B. Satpati, and T. Som, Appl. Surf. Sci. **418**, 225 (2017); R. Singh, M. Kumar, M. Saini, B. Satpati, and T. Som, Sol. Energy **174**, 231 (2018).
[18]W. Wang, H. Wang, W. Yang, Y. Zhu, and G. Li, Sci. Rep. **6**, 1 (2016).
[19]Y. Jiang, H. Shen, T. Pu, C. Zheng, Q. Tang, Y. Li, J. Wu, C. Rui, K. Gao, and Y. Liu, Sol. Energy **142**, 91 (2017).
[20]E. Vazsonyi, K. De Clercq, R. Einhaus, E. Van Kerschaver, K. Said, J. Poortmans, J. Szlufcik, and J. Nijs, Sol. Energy Mater. Sol. Cells **57**, 179 (1999).
[21]P. Campbell and M. A. Green, J. Appl. Phys. **62**, 243 (1987).
[22]H. Seidel, L. Csepregi, A. Heuberger, and H. Boumgrtel, J. Electrochem. Soc. **137**, 3626 (1990).
[23]Y. Jiang, H. Shen, C. Zheng, T. Pu, J. Wu, C. Rui, W. Yang, and Y. Li, Phys. Status Solidi A **214**, 1 (2017).
[24]P. Sana, L. Vázquez, R. Cuerno, and S. Sarkar, J. Phys. D Appl. Phys. **50**, 435306 (2017).
[25]H. Seidel, L. Csepregi, A. Heuberger, and H. Boumgrtel, J. Electrochem. Soc. **137**, 3612 (1990).
[26]K. Peng, M. Zhang, A. Lu, N. B. Wong, R. Zhang, and S. T. Lee, Appl. Phys. Lett. **90**, 1 (2007).
[27]L. Fesquet, S. Olibet, J. Damon-Lacoste, S. De Wolf, A. Hessler-Wyser, C. Monachon, and C. Ballif, in *2009 34th IEEE Photovoltaic Specialists Conference* (PVSC), *Philadelphia, PA, 7–12 June 2009* (IEEE, 2009), pp. 000754–000758.
[28]D. Iencinella, E. Centurioni, R. Rizzoli, and F. Zignani, Sol. Energy Mater. Sol. Cells **87**, 725 (2005).
[29]D. A. Kessler, H. Levine, and Y. Tu, Phys. Rev. A **43**, 4551(R) (1991).
[30]K.-S. Kim, J. A. Hurtado, and H. Tan, Phys. Rev. Lett. **83**, 3872 (1999).
[31]M. E. R. Dotto and M. U. Kleinke, Phys. Rev. B **65**, 245323 (2002).
[32]C. H. Lam and F. G. Shin, Phys. Rev. E **58**, 5592 (1998).
[33]See http://www.nanoscience.com/products/afm/afm-spip/ for AFM images analysis.
[34]See http://www.nanotec.es/products/wsxm/ for AFM images analysis.
[35]M. Hong, G. D. Yuan, Y. Peng, H. Y. Chen, Y. Zhang, Z. Q. Liu, J. X. Wang, B. Cai, Y. M. Zhu, Y. Chen, J. H. Liu, and J. M. Li, Appl. Phys. Lett. **104**, 253902 (2014).
[36]J. F. Sage, W. Barvosa-Carter, and M. J. Aziz, Appl. Phys. Lett. **77**, 516 (2000).
[37]Z. Mao and J. Chen, J. Chem. Eng. Sci. **59**, 1815 (2004).
[38]A. D'Aubeterre, R. Da Silva, and M. E. Aguilera, Int. Commun. Heat Mass Transf. **32**, 677 (2005).
[39]A. L. Barabási and H. E. Stanley, *Fractal Concepts in Surface Growth* (Cambridge University Press, Cambridge, 1995).
[40]H. S. Wio, C. Escudero, J. A. Revelli, R. R. Deza, and M. S. De La Lama, Philos. Trans. R. Soc. A **369**, 396 (2011).
[41]P. K. Dhillon and S. Sarkar, Appl. Surf. Sci. **284**, 569 (2013).
[42]X. Ou, K.-H. Heinig, R. Hübner, J. Grenzer, X. Wang, M. Helm, J. Fassbender, and S. Facsko, Nanoscale **7**, 18928 (2015).
[43]K. Imamura, T. Nonaka, Y. Onitsuka, D. Irishika, and H. Kobayashi, Appl. Surf. Sci. **395**, 50 (2017).

[44]M. Otto, M. Kroll, T. Käsebier, S. M. Lee, M. Putkonen, R. Salzer, P. T. Miclea, and R. B. Wehrspohn, Adv. Mater. **22**, 5035 (2010).
[45]X. Liu, P. R. Coxon, M. Peters, B. Hoex, J. M. Cole, and D. J. Fray, Energy Environ. Sci. **7**, 3223 (2014).
[46]H. Sai, Y. Kanamori, K. Arafune, Y. Ohshita, and M. Yamaguchi, Prog. Photovolt. Res. Appl. **15**, 415 (2007).
[47]S. Lee, H. Choo, C. Kim, E. Oh, D. Seo, and S. Lim, Appl. Surf. Sci. **371**, 129 (2016).
[48]S. Yun and T. Ji, Proc. SPIE **9742**, 97421Q-1 (2016).
[49]M. Zaknoune, O. Schuler, F. Mollot, D. Thèron, and Y. Crosnier, J. Vac. Sci. Technol. B **16**, 223 (1998).
[50]J. E. Carey, C. H. Crouch, R. Younkin, E. Mazur, M. Sheehy, and C. Friend, in *Proceedings of the 14th International Vacuum Microelectronics Conference (IVMC) 2001, Davis, CA, 12–16 August 2001* (IEEE, 2001), pp. 75–76.
[51]L. Chen, H. Yu, J. Zhong, C. Wu, L. Hu, and T. Zhang, IEEE Trans. Electron Devices **62**, 4305 (2015).
[52]T. Basu, M. Kumar, M. Saini, J. Ghatak, B. Satpati, and T. Som, ACS Appl. Mater. Interfaces **9**, 38931 (2017).
[53]T. Basu and T. Som, Appl. Surf. Sci. **418**, 340 (2017).
[54]S. Nandy, R. Thapa, M. Kumar, T. Som, N. Bundaleski, O. M. N. D. Teodoro, R. Martins, and E. Fortunato, Adv. Funct. Mater. **25**, 947 (2015).
[55]R. H. Fowler and L. Nordheim, Proc. R. Soc. Lond. A **119**, 173 (1928).
[56]Y. M. Fung, W. Y. Cheung, I. H. Wilson, D. Chen, J. B. Xu, S. P. Wong, and R. W. M. Kwok, J. Vac. Sci. Technol. B **19**, 884 (2001).
[57]C. Mu, Y. Yu, W. Liao, X. Zhao, D. Xu, X. Chen, and D. Yu, Appl. Phys. Lett. **87**, 113104 (2005).
[58]W. Zhao, R. Z. Wang, Z. W. Song, H. Wang, H. Yan, and P. K. Chu, J. Phys. Chem. C **117**, 1518 (2013).
[59]V. Zorba, P. Tzanetakis, C. Fotakis, E. Spanakis, E. Stratakis, D. G. Papazoglou, and I. Zergioti, Appl. Phys. Lett. **88**, 10 (2006).
[60]C. J. Park, D. K. Choi, J. Yoo, G. C. Yi, and C. J. Lee, Appl. Phys. Lett. **90**, 083107 (2007).
[61]D. K. Schroder, R. N. Thomas, J. Vine, and H. C. Nathanson, IEEE Trans. Electron Devices **21**, 785 (1974).
[62]H. C. Chang, C. C. Li, S. F. Jen, C. C. Lu, I. Y. yu Bu, P. W. Chiu, and K. Y. Lee, Diam. Relat. Mater. **31**, 42 (2013).